AMR Unit of Mineral Processing | ANTS Anthropogenic Material Cycles | RWTH AACHEN UNIVERSITY

SBSC 2022

9th Sensor-Based Sorting & Control

Kathrin Greiff,
Hermann Wotruba,
Alexander Feil,
Nils Kroell,
Xiaozheng Chen,
Devrim Gürsel,
Vincent Merz (eds.)

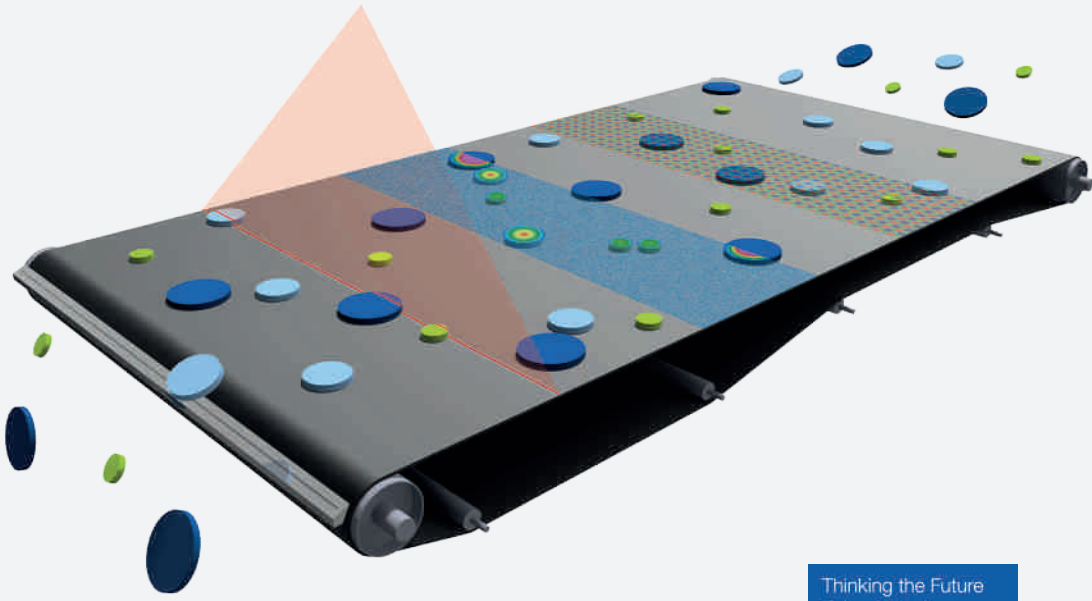

Thinking the Future
Zukunft denken

**Kathrin Greiff, Hermann Wotruba,
Alexander Feil, Nils Kroell, Xiaozheng Chen,
Devrim Gürsel, Vincent Merz (eds.)**

9th Sensor-Based Sorting & Control 2022

Shaker Verlag
Aachen 2022

Bibliographic information published by the Deutsche Nationalbibliothek
The Deutsche Nationalbibliothek lists this publication in the Deutsche Nationalbibliografie; detailed bibliographic data are available in the Internet at http://dnb.d-nb.de.

Printed in Germany.
Print-ISBN 978-3-8440-8516-7
PDF-ISBN 978-3-8440-8545-7
https://doi.org/10.2370/9783844085457

Shaker Verlag GmbH • Am Langen Graben 15a • 52353 Düren
Phone: 0049/2421/99011-0 • Telefax: 0049/2421/99011-9
Internet: www.shaker.de • e-mail: info@shaker.de

Assessment of sensor-based sorting performance for lightweight packaging waste through sensor-based material flow monitoring: Concept and preliminary results

Nils Kroell[1*], Tobias Dietl[1,2], Abtin Maghmoumi[1], Xiaozheng Chen[1], Bastian Küppers[2], Alexander Feil[1], Kathrin Greiff[1]

[1]Department of Anthropogenic Material Cycles, RWTH Aachen University, Aachen, Germany
[2]STADLER Anlagenbau GmbH, Altshausen, Germany
* Corresponding Author: Wüllnerstr. 2, D-52062 Aachen, Germany,
nils.kroell@ants.rwth-aachen.de

Keywords: sensor-based material flow monitoring, sensor-based sorting, sorting performance, post-consumer lightweight packaging waste, plastic recycling

Abstract

Background: Sensor-based sorting (SBS) units are a crucial part of lightweight packaging (LWP) waste sorting plants. Compared to sorting trials under technical lab conditions, significantly lower sorting performances are observed in many LWP sorting plants. One reason for this discrepancy is assumed to be the insufficient material flow representation under real sorting conditions. *Aim*: This paper aims to quantitatively determine how material flow presentation influences the performance of SBS units on the example of LWP waste. *Method*: In a case study, near-infrared (NIR) sensors were used to monitor the input, eject and drop fraction of an industrial-scale, NIR-based SBS unit at different troughputs. *Result*: Preliminary results show that higher occupation densities and insufficient material singling lead to significantly a lower sorting performance both in terms of purity of the eject fractions and yield of eject materials. *Conclusion*: The findings suggest that much of the discrepancy

between theoretically possible and practically achieved LWP sorting performance can be explained by suboptimal material flow presentation. Optimized material flow presentation thus might offer considerable, but so far largely untapped, optimization potentials in LWP sorting.

1 Introduction

Global plastic production has grown from 2 Mt to 380 Mt between 1950 and 2015 (Geyer et al., 2017) and is expected to double again over the next 20 years (European Commission, 2018). The current production, usage, and end-of-life disposal of plastics cause severe environmental damages, e.g., greenhouse gas (GHG) emissions (Zheng & Suh, 2019) and pollution of global ecosystems (Jambeck et al., 2015). Plastic recycling and the substitution of primary by recycled plastics can significantly lower the environmental impacts of plastics (Astrup et al., 2009; Perugini et al., 2005). For example, substituting 1 Mg of primary plastic with recycled plastic achieves GHG savings between 0.9 Mg and 2.2 Mg CO_2e (Turner et al., 2015).

Germany is the largest producer of post-consumer plastic waste in Europe and generated about 5.35 Mt/a post-consumer plastic wastes in 2019; the majority (59 wt%) of which is collected as post-consumer lightweight packaging (LWP) waste with an amount of 3.16 Mt/a (Conversio Market & Strategy GmbH, 2020). After collection, LWP waste is firstly sorted by LWP sorting plants into preconcentrates and a remaining sorting residue. Preconcentrates are further refined into secondary raw materials by specialized recycling plants and then re-enter the anthropogenic material cycle (Feil & Pretz, 2020). Although several improvements were introduced to LWP sorting (Feil et al., 2021), the overall performance of LWP sorting in Germany remains unsatisfactory: In 2019, only about 19 wt% of post-consumer plastic waste could be converted into recyclates, and only 8 wt% were used to substitute virgin material (Conversio Market & Strategy GmbH, 2020).

Considerable material losses towards energy recovery occur both during the collection with about 30 wt% as well as in sorting and recycling plants with about 35 - 40 wt% each of the respective inputs (Kuchta, 2020). As high material losses in recycling plants are partly caused by insufficient purity of preconcentrates (Dehoust & Christiani, 2012), technical optimization of LWP sorting plants plays a key role in improving the performance of post-consumer plastic recycling.

1.1 State of the art and challenges in LWP sorting

In LWP sorting plants, the input material flow is firstly preconditioned (liberation, sieving, wind-shifting, ballistic separation) before ferrous and non-ferrous metals as well as beverage cartons are sorted out. The preconditioned material flow then enters the heart of any modern LWP sorting plant: A sensor-based sorting (SBS) cascade typically containing more than 20 SBS units to sort the material flow into the desired preconcentrates. (Feil et al., 2021)

SBS units in LWP sorting are almost exclusively *belt sorters*, i.e., the material flow is presented on acceleration belts ($v \approx 3$ m/s) to the sensor. Compressed air nozzle bars are then used to sort the material flow in a *drop* and *eject* fraction, depending on the chosen sorting recipe. Common target fractions in SBS for LWP are polypropylene (PP), polyethylene (PE), polyethylene terephthalate (PET), polystyrene (PS), beverage cartons (BC), and paper & cardboard (PPC). As all target fractions of SBS in LWP have distinct near-infrared (NIR) spectra, NIR-based sorters are primarily used in LWP-sorting. (Feil et al., 2021; Feil & Pretz, 2020)

Modern SBS equipment can, according to manufacturers, achieve technical efficiencies of ≥ 95 wt% under laboratory and pilot plant conditions (4R Sustainability, 2011). However, the actual achieved product purities and observed material losses fall far short of these expectations (see above).

One main reason for the poor sorting results in industrial-scale LWP sorting is assumed to be the inadequate material flow presentation to the SBS unit (Feil et al., 2019): For optimal sorting results, material flows have to be presented as a *singled monolayer* to the SBS units. If particles overlap or touch each other, false-negative (material supposed to end in the eject fraction ends in the drop fraction) or false-positive (vice versa) sorting results occur, which lead to lower yield and purities, respectively. Two physically plausible mechanisms for false sorting results are:

(M1) **False sorting decisions due to overlapping:** All sensors currently applied in LWP sorting are *surface measurement technologies*. Thus, in the case of overlapping, only the material on top is considered in the sorting decision, leading to false-negative or false-positive sorting decisions, depending on the material on top. Additionally, mixed spectra (NIR) or colors (VIS) can lead to false sorting decisions in case the material on top is (semi-)transparent.

(M2) **Entrainment of drop particles:** In the case of overlapping or touching particles, turbulence of air valves can lead to false-positive material ejects (especially for light material fractions such as films).

1.2 Addressed research gap

This study aims to quantitatively determine how the material flow presentation influences the sorting results and how much of the discrepancy between theoretically possible and real-world observed sorting results can be explained by insufficient material flow presentation to SBS units in LWP sorting plants.

Recent studies have shown that the material throughput strongly influences the SBS performance of chute sorters in lab-scale (Küppers, Schlögl, et al., 2020; Küppers, Seidler, et al., 2020). However, the results are only partly transferable to industrial-scale SBS units since (i) LWP sorting is almost exclusively performed on belt sorters with significantly different feeding characteristics, (ii) the investigated working width (500 mm) is significantly lower compared to industrial applications (influence of boundary areas), and (iii) the characteristics of the investigated test material (idealized plastic chips) are not comparable with real-world post-consumer wastes. Additionally, investigations with industrial SBS equipment (Curtis et al., 2021) show that the throughput fluctuations hamper SBS performance but are limited to comparing two scenarios (fluctuating and non-fluctuating throughput).

One limitation of current SBS research is that existing performance assessment methods are based on manually determining the composition and quantity of eject and drop fractions (i.e., manual sorting), which is time- and cost-intensive. Therefore, only a small number of data points can be determined, limiting the statistical confidence of obtained results. Furthermore, sorting results are only available once the sorting trial is finished and therefore cannot be measured time-resolved and are limited to batch-wise trials. To overcome these limitations, we propose a new assessment method based on sensor-based material flow monitoring (SBMM), in which additional sensors are used to determine the composition and quantity of the eject and drop fractions.

2 SBS performance assessment based on SBMM

In the proposed assessment methodology, additional sensors are used to monitor (i) the material flow presentation on the acceleration belt and (ii) the sorting result, i.e., quantity and composition of the eject and drop fraction (Figure 1).

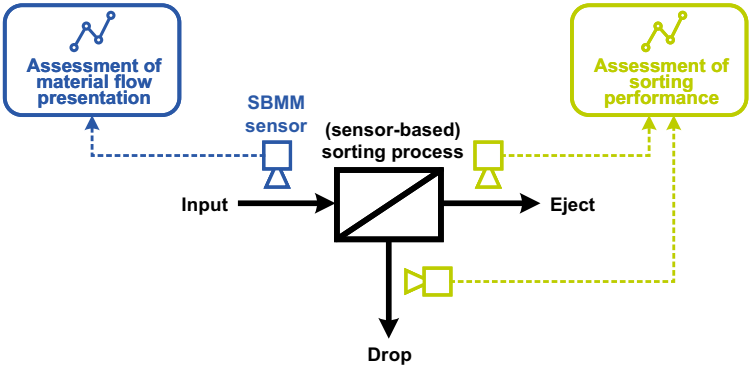

Figure 1: Concept for SBS performance assessment through SBMM.

2.1 Assessment of material flow presentation

To describe the material flow presentation on the acceleration belt quantitatively, this section define different material flow presentation indicators.

Occupation density (OD). Traditional assessment of material flow presentation of acceleration belts is based on the *occupation density* (OD), which describes the share of the acceleration belt area that is covered by material (Küppers, Schlögl, et al., 2020):

$$OD = \frac{\dot{A}_{\text{covered}}}{\dot{A}_{\text{belt}}} \qquad (1)$$

Where $\dot{A}_{\text{belt}}$ is the *area flow* (projected area per time unit as presented to the sensor) of the acceleration belt, which is a function of belt speed (v_{belt}) and belt width (b_{belt}) (Eq. (2)), and $\dot{A}_{\text{covered}}$ is the area flow of belt area that is covered by material.

$$\dot{A}_{\text{belt}} = v_{\text{belt}} * b_{\text{belt}} \qquad (2)$$

The OD can be calculated deterministically without prior knowledge about the material flow. However, as shown exemplarily in Figure 2, the OD neglects the material distribution on the conveyor surface (e.g., overlapping), which may influence the sorting result (see Mechanism M1, Section 1.1).

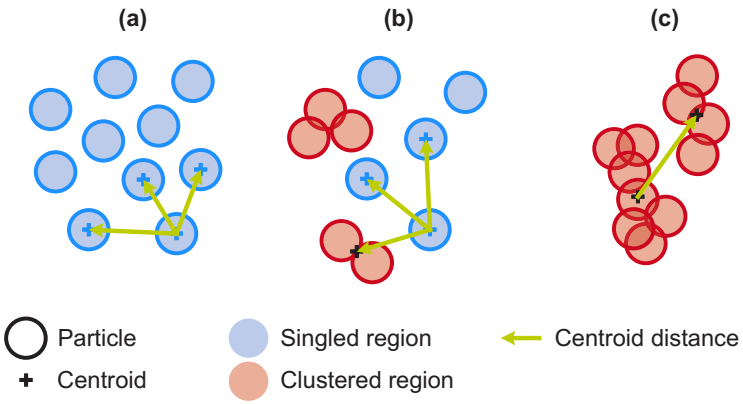

Figure 2: Exemplary material distributions with similar ODs, but (a) high, (b) medium, and (c) low particle singling.

Singling ratio (SR). To overcome the limitations of the occupancy density indicator, we propose a new indicator, the *singling ratio* (SR). To determine the SR, we classify all associated, covered areas (*regions*) into (i) *singled regions* (regions that contain only one particle) and (ii) *clustered regions* (regions that contain two or more touching or overlapping particles), cf. Figure 2. The SR then describes the percentage of covered area that is singled:

$$SR = \frac{\dot{A}_{\text{singled}}}{\dot{A}_{\text{singled}} + \dot{A}_{\text{clustered}}} = \frac{\dot{A}_{\text{singled}}}{\dot{A}_{\text{covered}}} \qquad (3)$$

A SR of 1 indicates perfect singling, while a SR of 0 means that all particles touch or overlap with at least one other particle.

Particle distances. While the SR describes the singulation of the material flow, it ignores the proximity to nearby regions, which may influence the sorting result (see Mechanism M2, Section 1.1). Different metrics can describe the distance between regions on a conveyor surface. Here, we use the Euclidian centroid-to-centroid distance between a given region i and its neighbor region j, where x and y are the coordinates of the respective centroid and region j is the k-th nearest neighbor of region i:

$$CD_k(i,j) = \sqrt{(x_i - x_j)^2 + (y_i - y_j)^2} \qquad (4)$$

On a material flow level, the distances of all n regions in a given evaluation area result in a distribution of individual centroids distances, which can be summarized through statistical indicators such as the arithmetic mean:

$$\overline{CD}_k = \frac{1}{n}\sum_{i=1}^{n} CD_{k,i} \qquad (5)$$

2.2 Assessment of sorting performance

In any SBS task, particles can be divided into target (index *T*) and non-target particles (index *nT*). Optimal sorting is defined by maximizing target and minimizing non-target particles in the eject fraction.

Four different sorting results can occur: (i) target material ends in the eject fraction ($\dot{m}_{\mathrm{T,eject}}$; true positive [TP]), (ii) target material ends in the drop fraction ($\dot{m}_{\mathrm{T,drop}}$; false-negative [FN]), (iii) non-target material ends in the drop fraction ($\dot{m}_{\mathrm{nT,drop}}$; true negative [TN]), and (iv) non-target material in the eject fraction ($\dot{m}_{\mathrm{nT,eject}}$; false-positive [FP]). Thus, the sorting result can be interpreted as a 2 x 2 confusion matrix:

$$\text{Confusion matrix: } \begin{bmatrix} \dot{m}_{\mathrm{T,eject}}\,(TP) & \dot{m}_{\mathrm{nT,eject}}\,(FP) \\ \dot{m}_{\mathrm{T,drop}}\,(FN) & \dot{m}_{\mathrm{nT,drop}}\,(TN) \end{bmatrix} \qquad (6)$$

Commonly, two indicators are used to evaluate the sorting task (Feil et al., 2016): *Purity* (Eq. (7)) describes the share of the target fraction in the eject fraction, i.e., evaluation of the first confusion matrix row.

$$c_{w,\mathrm{eject}} = \frac{\dot{m}_{T,\mathrm{eject}}}{\dot{m}_{\mathrm{eject}}} = \frac{\dot{m}_{T,\mathrm{eject}}}{\dot{m}_{\mathrm{T,eject}} + \dot{m}_{\mathrm{nT,eject}}} \quad (7)$$

Yield (Eq. (8)) describes how much of the target fraction from the input material flow is sorted into the eject fraction, i.e., evaluation of the first confusion matrix column.

$$R_{\mathrm{w}} = \frac{\dot{m}_{\mathrm{T,eject}}}{\dot{m}_{\mathrm{T,input}}} = \frac{\dot{m}_{\mathrm{T,eject}}}{\dot{m}_{\mathrm{T,eject}} + \dot{m}_{\mathrm{T,drop}}} \quad (8)$$

Although purity and yield are of high practical importance, both indicators must always be considered to evaluate the sorting performance. To obtain a single performance indicator, we propose to unite purity and yield into the F_1-score, which is the harmonic mean of both values (Tharwat, 2021):

$$F_1 = 2 \cdot \frac{c_{\mathrm{w,eject}} \cdot R_{\mathrm{w}}}{c_{\mathrm{w,eject}} + R_{\mathrm{w}}} \quad (9)$$

F_1-scores range between 0 and 1. An F_1-score of 1 indicates a perfect sorting performance ($c_{\mathrm{w,eject}}$ and R_{w}=1),), while the F_1-score becomes zero if purity or yield become zero.

In cases where purity and yield are not of equal importance, it is possible to weigh both indicators through a factor β in the F_β-score (Eq. (10)), which leads to yield being weighted β-times more than purity (Tharwat, 2021).

$$F_\beta = (1 + \beta^2) * \frac{c_{w,\mathrm{eject}} \cdot R_{\mathrm{w}}}{(\beta^2 \cdot c_{w,\mathrm{eject}}) + R_{\mathrm{w}}} \quad (10)$$

3 Case study: Material and methods

In a case study, we tested the technical feasibility of our assessment method with an industrial scale SBS unit using real-world LWP waste.

3.1 Test setup

The developed test setup consists of a state-of-the-art, industrial-scale NIR-based SBS unit with a total working width of 2000 mm, an acceleration belt speed of 3 m/s, and an air nozzle bar with 12.5 mm nozzle distance operated at 5.5 bar air pressure. For the sorting trials, the effective working width was reduced to 1000 mm to enable high occupation despite the limited transport capacity of the upstream conveyors. The sorter was programmed to actively sort out PET, while all other materials were supposed to end in the drop fraction. The sorting recipe came directly from the SBS manufacturer, represented an industry-standard sorting recipe used in several LWP sorting plants, and was not further modified or adapted for the sorting trials.

A first additional NIR sensor (NIR-1) recorded the acceleration belt. After the SBS unit, the drop and eject fraction then fell on separate conveyor belts respectively (width: b = 830 mm, belt speed: v = 1.2 m/s), where both material flows were captured by a second NIR sensor (NIR-2). Afterward, the NIR-2 recordings were digitally split into eject and drop recordings. To simulate a continuously working sorting plant, eject and drop material flows were mixed and entered a material loop before being fed again to the SBS unit. Inside the material loop, a modified ballistic separator and several belt transfers ensured a material flow homogenization before re-entering the SBS units.

The used NIR sensors were EVK HELIOS EQ32 sensors from EVK Kerschhaggl GmbH (Raaba, Austria) working in the wavelength range of 930 nm – 1700 nm with a spectral resolution of 3.1 nm at an acquisition frequency of 450 Hz. An analysis recipe (Figure 3a) containing spectral references for the material classes PET, PP, PE, PS, BC, and PPC was developed and loaded on both NIR sensors. The NIR sensors classify each pixel based on the analysis recipe, and the resulting false-color images (Figure 3b-d) were recorded using a self-developed recording software for subsequent data analysis.

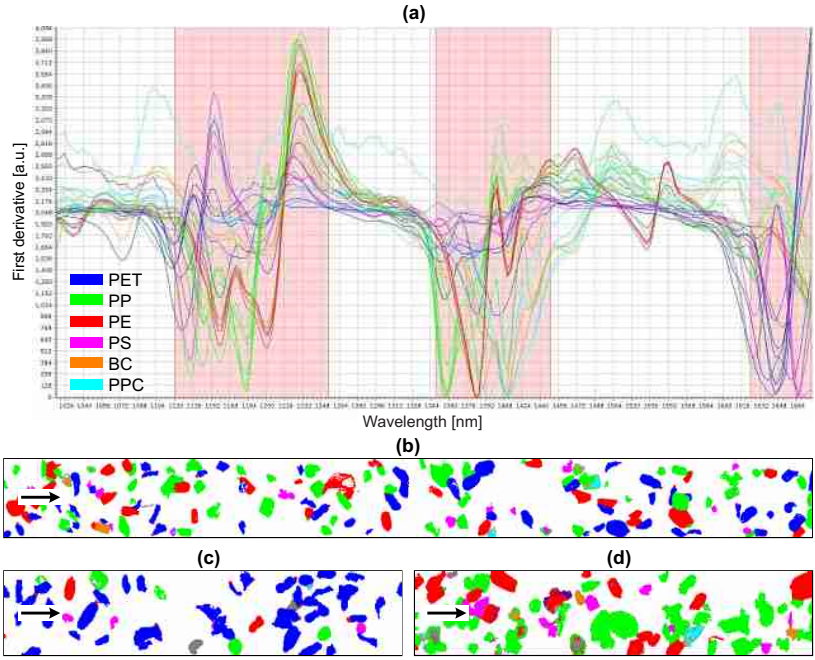

Figure 3: (a) NIR recipe and resulting false-color images (red marked areas are used for spectral classification) of (b) acceleration belt (NIR-1), (c) eject, and (d) drop belt (NIR-2). Grey: unclassified material.

3.2 Material and experimental procedure

The investigated test material is LWP waste from Maribor (Slovenia). To simulate a realistic 3D plastic fraction typical for SBS applications in LWP sorting, we preconditioned the material flow before the trials with a ballistic separator to remove 2D materials and fines (< 45 mm) and an eddy current and magnetic separator to remove ferrous and non-ferrous metals, respectively. To achieve material flow with a certain percentage of eject material (in this case PET), pure PET and non-PET fractions were generated firstly. For the PET fraction, post-consumer PET bottles were used as the source material. To ensure proper classifiability of each bottle and to exclude false discharges due to poor classifiability of certain bottles (e.g., full-sleeve bottles), the PET fraction was delabeled with the STADLER Delabeler

(Küppers et al., 2019) to generate a pure post-consumer PET fraction and exclude the influences of labels and sleeves on the sorting result. A non-PET 3D plastic fraction was generated by sorting out all PET contents from the preconditioned LWP waste prior to the sorting trials. Subsequently, a PET content of 30 wt% was set for the test material by mixing defined amounts of the PET and non-PET fraction.

Different material flow presentations were simulated by gradually increasing the throughput in 16 throughput steps. The throughput increases were achieved by adding a defined amount of additional test material to the material loop in each step. After a buffer time of 5 minutes to equilibrate the material loop, the sorting results were monitored for 10 minutes (equivalent to about 3.5 material cycles) for each throughput step.

3.3 Data evaluation

The subsequent data analysis was implemented in Python 3.8. First, all images were spatially calibrated to obtain results in metric units. Second, the material flow composition and OD were determined and aggregated to a sampling rate of 15 Hz. Third, each region was classified into singled and clustered regions, and centroid distances were determined. After that, the SR was determined, and the centroid distances were resampled by evaluating the image in chunks of 1/15 s length in conveying direction. To reduce the artifacts of individual particles and obtain information on the material flow level, all results were smoothed by a 1s moving average.

The sorting performance indicators (Eq. (11)-(13)) were then calculated by comparing the area flows per material class:

$$c^*_{\mathrm{PET,eject}} = \frac{\dot{A}_{\mathrm{PET,eject}}}{\dot{A}_{\mathrm{eject}}}\ [\mathrm{px\%}] \tag{11}$$

$$R^*_{\mathrm{PET}} = \frac{\dot{A}_{\mathrm{PET,eject}}}{\dot{A}_{\mathrm{PET,eject}} + \dot{A}_{\mathrm{PET,drop}}}\ [\mathrm{px\%}] \tag{12}$$

$$F_{1\,\mathrm{PET}}{}^{*} = 2 \cdot \frac{c^*_{\mathrm{PET,eject}} \cdot R^*_{\mathrm{PET}}}{c^*_{\mathrm{PET,eject}} + R^*_{\mathrm{PET}}}\ [\mathrm{px\%}] \tag{13}$$

For a mass-based process evaluation, these area-based indicators have to be transformed into mass-based indicators (Kroell et al., 2021), which we plan to address in future work. Since the grammages of the investigated material groups are in a similar order of magnitude, we neglect this effect for the first demonstration of technical feasibility and report the preliminary results in pixel percent (px%), cf. Eq. (11) – Eq. (13).

4 Case study: Preliminary results and discussion

4.1 Discrimination of singled and clustered regions

To determine if the classification into singled and clustered regions based on the NIR-1 recordings (false-color images) is technically feasible, we manually classified n = 1,000 randomly sampled regions. The resulting dataset contained n = 632 (63.2%) singled, n = 335 (33.5%) clustered regions, and n = 33 (3.3%) regions that could not be classified unambiguously (which were excluded from the labeled dataset).

For an initial classifier, we extracted the two features (i) *impurity* (share of all except the most common material classes and unclassified material of a particle) and (ii) *projection area* of each region and split the dataset into 75% training and 25% test data. Figure 4 shows the distribution of impurities and projection areas between the singled and clustered regions.

Based on the training data, we determined two thresholds (i) τ_{impurity} = 12 px% (optimal threshold between singled and clustered regions, see Figure 4a) and (ii) τ_{area} = 1,000 cm² (maximum projection area of singled clustered incl. 10% buffer for different particle positions). Based on these thresholds, we constructed a simple if/else classifier:

$$RT = \begin{cases} \text{"clustered"}, if\ I_{\text{region}} \geq \tau_{\text{impurity}} \text{ or } A_{\text{region}} \geq \tau_{\text{area}} \\ \text{"singled"}, else \end{cases} \quad (14)$$

Where I_{region} and A_{region} are the impurity and projection area of a region respectively, and RT is the region type. Figure 4c shows that this simple classifier already achieves a classification accuracy of 92.3% and can sufficiently discriminate singled from clustered regions (Figure 4d).

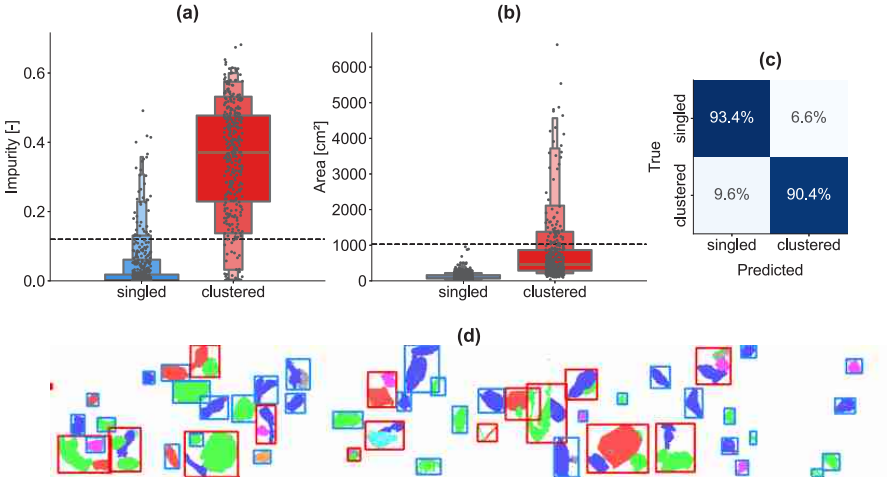

Figure 4: Identification of clustered regions. (a) Distribution of material impurities per region type, (b) distribution of projection areas per region type, (c) confusion matrix of region type classification based on impurity and projection area thresholds (dashed line in [a] and [b]) and or-conjunction on the test set, (d) exemplary false-color image with identified regions (blue: singled, red: clustered).

The classification accuracy can likely be improved by incorporating more features, extending the training data set, and applying sophisticated machine learning (ML) models. Especially convolutional neural networks (CNNs) could be promising for this classification task.

4.2 Interrelation between material flow presentation indicators

Based on the discrimination of singled and clustered regions, the SR was calculated, and Figure 5a shows the interrelation between OD, SR and relative throughput. As one would expect, the OD increases with increasing relative throughput, while the SR decreases. Two segments can be identified: For ODs between 0% and about 20%, the SR stays roughly constant. For ODs above about 20%, the SR decreases with increasing belt occupation.

The centroid distances (Figure 5b) decrease with increasing OD, i.e., regions move closer together. However, at ODs above about 30%, increased region distances can be observed. This effect can be very likely be traced back to the formation of more clustered regions (cf. Figure 5a) at higher ODs: As the clustered regions have

larger projection areas than singled particles, the centroid distances increase with lower SRs and higher ODs.

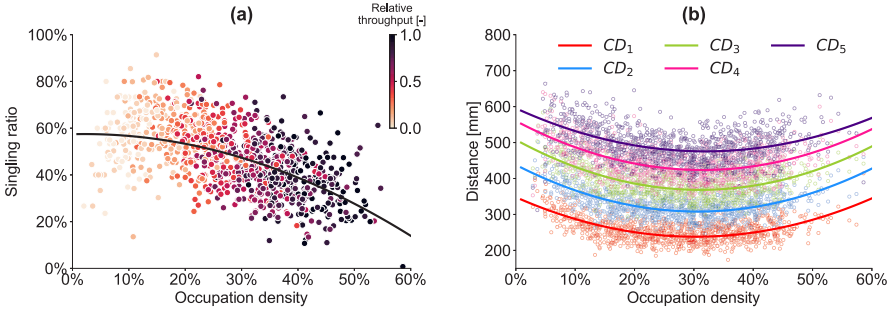

Figure 5: Interrelation between (a) OD and SR for different relative throughputs and (b) OD and centroid distances. CD_i: centroid distance to i-th nearest neighbor. (1s moving average; scatterplot for better visualization limited to a random selection of 1,000 data points each)

These findings show that the SR can be a useful metric to assess the material flow presentation besides the OD. However, as all sorting trials were conducted on the identical acceleration belt and with identical material flow guidance, the additional advantage of SR over the OD can currently only be estimated to a limited extent.

Furthermore, the prelimary SBMM data indicates that the presentation of post-consumer LWP as a singled monolayer to SBS units is indeed challenging: Even at the lowest investigated throughputs (mean OD: 8.8%), only about half of the covered area (mean SR: 52.4%) was classified as singled.

In contrast, the centroid-to-centroid distances seem to be of limited use for describing the particle proximity at higher ODs due to the formation of clusters. Here, region distances that describe the distances between individual region borders could be a potential improvement.

4.3 Influence of material flow presentation on sorting performance

Figure 6 shows the interrelation between the material flow presentation (assessed by the OD and SR) and different sorting performance metrics (purity, yield, -score). As depicted in Figure 6a, the sorting performance decreases linearly with increasing OD from about 91.6 px% purity and 98.7 px% yield at 8.8% OD to about 74.2 px% purity and 97.0 px% yield at 42.6% OD.

For the investigated SBS unit, a 12.2-fold steeper decrease of the purity with increasing OD (slope: -0.49) compared to the yield (slope: -0.04) can be observed. Accordingly, Figure 6b shows an increased sorting performance for higher SR. Here, the purity increases 12.5 times steeper than the purity with increasing SR. As graphically shown in Figure 6, the -score can be a useful performance metric to combine purity and yield.

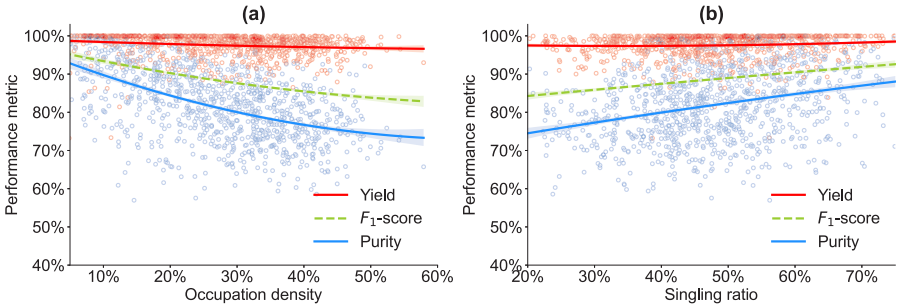

Figure 6: Influence of (a) OD and (b) SR on sorting performance. (5s moving average; scatterplot for better visualization limited to a random selection of 1,000 data points each)

The significantly reduced sorting performance of SBS units due to suboptimal material flow presentation (high OD) is consistent with related research (Curtis et al., 2021; Küppers, Schlögl, et al., 2020; Küppers, Seidler, et al., 2020). In contrast, a quantitative comparison of our findings with the results of Küppers, Seidler, et al. (2020) highlights the significant influence of individual SBS units, machine settings, and material flows on the obtained transfer function (quantitative relation between material flow presentation or throughput and sorting result): While Küppers, Seidler, et al. (2020) report a decreased yield of on average -0.76% per 1% additional OD, the yield of our investigated SBS unit decreased with only -0.04% per 1% additional OD. A possible explanation for this is that in state-of-the-art SBS equipment, the weighting of purity and yield can be adjusted in the sorter settings, and changing these weightings would directly affect the slope of the purity and yield in the obtained transfer function. Moreover, the sorting results are influenced by the characteristics of the underlying sorting engine and the input material. It would thus be interesting to compare the sorting performance as assessed through the -score for different SBS settings or different SBS units in future work.

4.4 Limitations

It is essential to note that the obtained purity and yield values cannot be directly transferred to plant scale LWP sorting due to (i) the pixel-based performance assessment (cf. Section 3.3) and (ii) the removal of articles with limited sortability (cf. Section 3.2). The first limitation (pixel-based assessment) results in underestimating the sorting performance, as, e.g., PE bottle caps on PET bottles are counted as target material in traditional (particle-based) sorting assessment, but as non-target material in our pixel-based assessment method. The second limitation causes overestimating of the sorting performance, as articles with limited sortability would cause additional sorting errors. Here, a direct comparison of the SBMM- and pixel-based sorting assessment with traditional (particle-based) performance assessment would be of great value.

5 Conclusion and outlook

In conclusion, our case study shows that an automatic assessment of (sensor-based) sorting processes is technically feasible and offers significant advantages over state-of-the-art assessment methods, e.g., in terms of reduced time and cost expenditure, a higher statistical significance of the results, and greater flexibility and detail of data evaluation. The introduced indicators singling ratio and particle distances enable a more nuanced description of the material flow presentation and demonstrate the difficulty of singling post-consumer LWP wastes on acceleration belts.

Our results show that increased belt occupation significantly linearly reduces the sorting performance of SBS equipment in terms of lower purity, yield, and overall sorting performance (F_1-score). These preliminary findings suggest that much of the discrepancy between theoretically possible and practically achieved LWP sorting performance can be explained by suboptimal material flow presentation.

In future work, we plan to extend the sorting trials to different material flow compositions and further improve the developed assessment method. Furthermore, the hypothesis that large parts of the discrepancy between theoretically possible and practically achieved LWP sorting performance can be explained by suboptimal material flow presentation shall be investigated in SBMM trials at plant scale. If this hypothesis is validated, optimized material flow presentation offers considerable,

but so far largely untapped, optimization potential in LWP sorting and could largely contribute to a loss-minimized plastic recycling in general.

Acknowledgments

This work was supported by the German Federal Ministry of Education and Research (BMBF) within the program „Resource-efficient circular economy - plastics recycling technologies (KuRT)“ under the project ReVise (grant no. 033R341).

References

4R Sustainability, I. (Ed.). (2011). *Demingling the mix: An assessment of commercially available automated sorting technology.*

Astrup, T., Fruergaard, T., & Christensen, T. H. (2009). Recycling of plastic: Accounting of greenhouse gases and global warming contributions. *Waste Management & Research*, *27*(8), 763–772. https://doi.org/10.1177/0734242X09345868

Conversio Market & Strategy GmbH. (2020). *Stoffstrombild Kunststoffe in Deutschland 2019.*

Curtis, A., Küppers, B., Möllnitz, S., Khodier, K., & Sarc, R. (2021). Real time material flow monitoring in mechanical waste processing and the relevance of fluctuations. *Waste Management (New York, N.Y.)*, *120*(1), 687–697. https://doi.org/10.1016/j.wasman.2020.10.037

Dehoust, G., & Christiani, J. (2012). *Analyse und Fortentwicklung der Verwertungsquoten für Wertstoffe: Sammel- und Verwertungsquoten für Verpackungen und stoffgleiche Nichtverpackungen als Lenkungsinstrument zur Ressourcenschonung*. http://www.uba.de/uba-info-medien/4342.html

European Commission (Ed.). (2018). *A European Strategy for Plastics in a Circular Economy*. https://eur-lex.europa.eu/legal-content/EN/TXT/?uri=COM:2018:28:FIN

Feil, A., Coskun, E., Bosling, M., Kaufeld, S., & Pretz, T. (2019). Improvement of the recycling of plastics in lightweight packaging treatment plants by a process control concept. *Waste Management & Research*, *37*(2), 120–126. https://doi.org/10.1177/0734242X19826372

Feil, A., Kroell, N., Pretz, T., & Greiff, K. (2021). Anforderungen an eine effiziente technologische Behandlung von Post-Consumer Verpackungsmaterialien in Sortieranlagen. *Müll Und Abfall*, *21*(7), 362–370. https://doi.org/10.37307/j.1863-9763.2021.07.04

Feil, A., & Pretz, T. (2020). Mechanical recycling of packaging waste. In *Plastic Waste and Recycling* (pp. 283–319). Elsevier. https://doi.org/10.1016/B978-0-12-817880-5.00011-6

Feil, A., van Thoden Velzen, E. U., Jansen, M., Vitz, P., Go, N., & Pretz, T. (2016). Technical assessment of processing plants as exemplified by the sorting of beverage cartons from lightweight packaging wastes. *Waste Management (New York, N.Y.)*, *48*, 95–105. https://doi.org/10.1016/j.wasman.2015.10.023

Geyer, R., Jambeck, J. R., & Law, K. L. (2017). Production, use, and fate of all plastics ever made. *Science Advances*, *3*(7), e1700782. https://doi.org/10.1126/sciadv.1700782

Jambeck, J. R., Geyer, R., Wilcox, C., Siegler, T. R., Perryman, M., Andrady, A., Narayan, R., & Law, K. L. (2015). Marine pollution. Plastic waste inputs from land into the ocean. *Science (New York, N.Y.)*, *347*(6223), 768–771. https://doi.org/10.1126/science.1260352

Kroell, N., Chen, X., Maghmoumi, A., Koenig, M., Feil, A., & Greiff, K. (2021). Sensor-based particle mass prediction of lightweight packaging waste using machine learning algorithms. *Waste Management (New York, N.Y.)*, *136*, 253–265. https://doi.org/10.1016/j.wasman.2021.10.017

Kuchta, K. (2020). Bewertung des Recyclingprozesses von Kunststoffverpackungen. In O. Holm, E. Thomé-Kozmiensky, D. Goldmann, & B. Friedrich (Chairs), *Recycling- und Sekundärrohstoffe,* Berlin.

Küppers, B., Chen, X., Seidler, I., Friedrich, K., Raulf, K., Pretz, T., Feil, A., Pomberger, R., & Vollprecht, D. (2019). Influences and consequences of mechanical delabeling on PET recycling. *Detritus*, *6*(0), 39–46. https://doi.org/10.31025/2611-4135/2019.13816

Küppers, B., Schlögl, S., Friedrich, K., Lederle, L., Pichler, C., Freil, J., Pomberger, R., & Vollprecht, D. (2020). Influence of material alterations and machine impairment on throughput related sensor-based sorting performance. *Waste Management & Research.* Advance online publication. https://doi.org/10.1177/0734242X20936745

Küppers, B., Seidler, I., Koinig, G. R., Pomberger, R., & Vollprecht, D. (2020). Influence of throughput rate and input composition on sensor-based sorting efficiency. *Detritus*(9), 59–67. https://doi.org/10.31025/2611-4135/2020.13906

Perugini, F., Mastellone, M. L., & Arena, U. (2005). A life cycle assessment of mechanical and feedstock recycling options for management of plastic packaging wastes. *Environmental Progress*, *24*(2), 137–154. https://doi.org/10.1002/ep.10078

Tharwat, A. (2021). Classification assessment methods. *Applied Computing and Informatics*, *17*(1), 168–192. https://doi.org/10.1016/j.aci.2018.08.003

Turner, D. A., Williams, I. D., & Kemp, S. (2015). Greenhouse gas emission factors for recycling of source-segregated waste materials. *Resources, Conservation and Recycling*, *105*, 186–197. https://doi.org/10.1016/j.resconrec.2015.10.026

Zheng, J., & Suh, S. (2019). Strategies to reduce the global carbon footprint of plastics. *Nature Climate Change*, *9*(5), 374–378. https://doi.org/10.1038/s41558-019-0459-z